Lasers in Surgery and Medicine 21:235–247 (1997)

Control of Fibroblast Populated Collagen Lattice Contraction by Antibody Targeted Photolysis of Fibroblasts

Louis H. Strong, PhD, Francois Berthiaume, PhD, and Martin L. Yarmush, MD, PhD*

Center for Engineering in Medicine/Surgical Services, Massachusetts General Hospital and Department of Surgery, Shriners Burns Institute, Harvard Medical School, Boston 02114

Background and Objective: **Hypertrophic scarring and rigid scar contracture are disorders of wound healing for which there is presently no effective therapy. The dermal fibroblast plays a major role in scar fibrillogenesis and contracture. The objective of this study was to establish a selective and effective method to destroy fibroblasts.**

Study Design/Materials and Methods: **An antifibroblast conjugate was synthesized by covalent attachment of the antifibroblast antibody PR2D3 to the photosensitizer Sn-chlorin e6. Fibroblasts were cultured in fibroblast-populated collagen lattices (FPCLs), incubated with the conjugate and exposed to light. The effect of the treatment on cell viability and the rate of contraction of the FPCL were assessed.**

Results: **The toxicity of antifibroblast conjugates increased with increasing conjugate concentration, light dose, and number of photosensitizers per antibody molecule, until nearly complete killing was achieved. The rate of lattice contraction after irradiation linearly correlated with the remaining viable fraction of fibroblasts. These conjugates were not cytotoxic to keratinocytes cultured on collagen lattices, and nonspecific conjugates could not cause significant fibroblast killing. Spatial selectivity was demonstrated using a light mask.**

Conclusions: **Antibody-targeted photolysis is an effective and selective technique for controlling FPCL contraction in vitro and may have potential in vivo applications to modulate extracellular matrix remodeling by connective tissue cells. Lasers Surg. Med. 21:235–247, 1997.** **© 1997 Wiley-Liss, Inc.**

Key words: hypertrophic scarring; scar contracture; wound contraction

INTRODUCTION: CONTROLLING WOUND CONTRACTION

Excessive wound contraction can lead to a significant impairment in joint motion and disfigurement. Current therapies aimed at limiting wound contraction and severe scarring include the use of compressive garments, topical silicone sheets, intralesional injection of steroids, and surgical excision of scar tissue followed by grafting [1,2]. These therapies are generally moderately effective, do not selectively target the putative agents of the contraction process, and affect wound healing via unknown mechanisms. It has been hypothesized that wound contraction is mediated by fibroblasts and myofibroblasts that exert tensile forces on the surrounding matrix in the collagenous connective tissue of the skin [3]. A

Contract grant sponsors: The Shriners Hospital for Crippled Children and the Lucille P. Markey Charitable Trust.

*Correspondence to Martin L. Yarmush, M.D., Center for Engineering in Medicine, Bigelow 1401, Massachusetts General Hospital, 55 Fruit Street, Boston, MA 02114.

Accepted 23 January 1997

useful cell culture model for studying the interaction between these connective tissue cells and the extracellular matrix is the fibroblast populated collagen lattice (FPCL), originally described by Bell et al. [4]. FPCLs are created by embedding fibroblasts in a uniform three-dimensional Type I collagen lattice. The collagen lattice rapidly undergoes a reduction in diameter that is similar to that seen during wound contraction. The contraction rate is inversely proportional to the concentration of collagen and proportional to the number of cells in the lattice [4,5].

FPCLs are potentially useful to study the effect of therapeutic agents or modalities that could modulate wound contraction. We and others have previously reported a cell killing approach called antibody targeted photolysis (ATPL), which uses conjugates consisting of a monoclonal antibody (mAb) covalently attached to a photosensitizer (PS) molecule. Conjugates against bacteria [6–10] and mammalian cells [11–26] have exhibited specific and effective killing both in vitro and in vivo. ATPL exhibits two levels of selectivity. First, the mAb binds to the target cell via specific cell surface receptors. This proximity of the conjugate to the target is required for killing because of the short range of action of the PS (100 nm or less). The second aspect of the selectivity involves limiting the illumination field and controlling the timing of illumination.

In the current study, we have synthesized PS-containing immunoconjugates that specifically bind fibroblasts cultured in FPCLs and demonstrate that these conjugates, in combination with light, cause effective killing of fibroblasts. By altering various input parameters, we also show that the extent and rate of FPCL contraction could be modulated. Finally, the spatial distribution of cell killing could be precisely controlled, thereby illustrating the high degree of spatial selectivity provided by this technique. These results show that ATPL is a potentially useful tool to modulate extracellular matrix contraction by connective tissue cells.

MATERIALS AND METHODS

The PR2D3 mAb is an IgG_1 produced from a mouse hybridoma cell line kindly supplied by Sir Walter Bodmer (Imperial Cancer Center Research Fund, London, UK) [29]. This antibody has been found to bind a 140 kD surface glycoprotein on pericrypt sheath cells and myofibroblasts in colorectal mucosa and cross reacts with vascular smooth muscle cells [29]. An anti-*Pseudomonas aeruginosa* IgG_1 was purchased from Xoma Corporation (Berkeley, CA; lot #50409). Chlorin e_6 was purchased from Porphyrin Products (Logan, UT). Stannous chloride was from MCB Manufacturing Chemists (Cincinnati, OH). Smooth muscle cells from the muscularis propria of the human jejunum (1692-CRL) and normal human skin fibroblasts (1784-CRL, passages 6–9) were obtained from the American Type Culture Collection (ATCC) as cryopreserved cells. Normal human neonatal epidermal keratinocytes (CC2503) were purchased from Clonetics (San Diego, CA) as primary cultures. Dulbecco's modified essential medium (DMEM), RPMI 1640 medium, sodium pyruvate, L-glutamine, penicillin-streptomycin 100 X stock solution, fetal bovine serum (FBS), and trypsin were all purchased from Sigma Chemical (St. Louis, MO) and Gibco (Gaithersburg, MD). Bacterial collagenase was purchased from Boehringer Mannheim, (Mannheim, Germany). Calcein acetoxymethyl ester (calcein AM) and ethidium homodimer were obtained from Molecular Probes (Eugene, OR). All other chemicals were from Sigma Chemical. Deionized water was produced using a Milli-Q unit from Millipore (Bedford, MA). All solvents were reagent grade.

Preparation and Characterization of mAbs

The hybridoma cell line was cultured in spinner flasks at 10^5 cells/mL in RPMI 1640 medium supplemented with 10% FBS and 5% penicillin-streptomycin stock solution. Half of the cell suspension was withdrawn weekly and replaced with fresh medium. The harvested cell suspensions were centrifuged and supernatants stored at −20°C until further use. The PR2D3 mAb was purified from the supernatants by precipitation in ammonium sulfate followed by chromatography on Affi-Gel Blue (Biorad, Hercules, CA) to remove serum proteins and finally on a protein G affinity column. The binding constant of the PR2D3 antibody for smooth muscle cells was found to be 1×10^9 M^{-1} based on an ELISA determination performed as described elsewhere [32]. The binding constant of the anti-*P. aeruginosa* mAb as supplied was previously determined by radioimmunoassay to be 5×10^8 M^{-1} [10].

Preparation of Bis(triethanolamine) Sn(IV) Chlorin e6 Ethylenediamine-mAb Conjugates

The detailed synthesis, biological, and physico-chemical characterization of similar immunoconjugates are described elsewhere [8,10]. Briefly, the PS dye Sn(IV) chlorin e_6 was cova-

lently linked to the oligosaccharide moiety on the Fc portion of the PR2D3 mAb via an ethylenediamine linker. Triethanolamine was used as the axial ligand to the Sn(IV) chlorin e_6. A bulky axial ligand was found necessary to preserve PS integrity in plasma [10]. HPLC analysis of the final product was performed with a Beckman System Gold Chromatograph equipped with a model 167 scanning detector, using a TSK 3000SW column and a mobile phase of 0.1 M phosphate buffer/0.1 M sodium sulfate, pH 6.2. A single peak corresponding to a molecular weight range of 140–160 kD was obtained. PR2D3-Sn(IV) chlorin e_6 conjugates were synthesized with loadings of 0.5, 1.0 and 2.0 PS/mAb. Anti-*P. aeruginosa*-PS conjugates with loadings of 1.4, 2.7, and 3.5 PS/mAb were synthesized using similar methods. The number of PS per molecule of mAb is based on the ratio of absorbances at 409 nm (PS) and 280 nm (protein) as measured on a Beckman DU-65 spectrophotometer.

Cell Culture and Collagen Contraction Measurement

Fibroblasts (1784-CRL) were cultured in DMEM supplemented with 1 mM sodium pyruvate, 4 mM L-glutamine, 10% FBS, and 1% penicillin-streptomycin stock solution in standard tissue culture flasks. FPCLs were constructed from rat tail Type I collagen according to the procedure of Bell et al. [4,5]. Type I rat tail tendon collagen in 1 mM HCl (2.1 mg/mL) was prepared as described elsewhere [33] and stored at 4°C until use. Nine parts of this collagen solution were neutralized with one part of 10 X concentrated DMEM on ice. The fibroblasts were removed from the plastic substrata by trypsin digestion and a 1 mL cell suspension containing 10^5 cells was mixed with 1.3 mL of the neutralized collagen solution. The suspension was allowed to gel in a 35 mm bacterial culture Petri dish (not tissue culture treated) at 37°C for 12–14 hr. The collagen lattice was detached from the dish surface by gentle swirling of the gel, and 1 mL of supplemented DMEM was added. Medium was replaced every third day. To measure lattice contraction, the FPCL was visualized through a 4X objective on a Nikon inverted microscope equipped with a translation stage that contained a vernier indicator. Lattice diameters were measured daily along two orthogonal directions and averaged. In some cases, FPCLs were overlaid with human keratinocytes. Fetal foreskin keratinocytes were maintained in serum-free Keratinocyte Growth Medium from Clonetics. 10^5 keratinocytes were seeded onto 1-day-old FPCLs and these FPCLs were maintained in serum-free Keratinocyte Growth Medium until use (2 more days). At that time, keratinocytes were 20–30% confluent on the surface of the FPCL. The lack of keratinocyte penetration into the interior of the FPCL together with their colony clustering and cobblestone appearance made it easy to visually distinguish keratinocytes from fibroblasts in situ.

Measurement of Cellular Uptake of mAbs by Fibroblasts in FPCLs

PR2D3 and anti-*P. aeruginosa* mAbs were radiolabeled with ^{125}I using Bolton-Hunter reagent (Dupont-NEN, Billerica, MA) [34]. During iodination, the pH was maintained at 8.5 and the reaction allowed to proceed for 30 min at 0°C. The trichloroacetic acid-precipitable fraction contained >95% of the radioactivity. The specific activities of the radiolabeled PR2D3 and anti-*P. aeruginosa* mAbs were 4.5×10^{16} and 1.2×10^{16} cpm/mol, respectively. After FPCLs were cultured for 3 or 8 days, culture medium was removed. DMEM supplemented with 50% FBS was added and allowed to incubate for 1 hr. This medium was then removed and replaced by radiolabeled mAb (final concentration = 0–1,000 nM, taking into account gel volume), which was in DMEM supplemented with 50% FBS. After 16 hr at 37°C, the mAb solution was removed, fresh DMEM + 10% FBS added, and the FPCL was incubated for 0.5 hr under gentle agitation. The lattices were washed twice more with fresh DMEM, followed by Krebs-Henseleit buffer containing 15 mM Hepes and 2.5 mM $CaCl_2$, pH 7.4. One mL of Krebs-Henseleit buffer with 0.1% collagenase was added, and after incubation for 20–30 min at 37°C, the dissolved FPCL along with the collagenase solution was centrifuged at 100 × g for 5 min. The pellet was washed three times and its radioactivity determined in a gamma counter (Wallac Model 1470, Gaithersburg, MD). The radioactivity of the collagenase digest supernatant was also measured and accounted for <10% of the total radioactivity in the FPCL (cell pellet + supernatant). Radioactivity data were normalized to total cell number in each FPCL. The cell number was determined by lysing the cell pellet in 1 mL of Tris buffer (100 mM, pH = 7.4) containing 1 mM EDTA and 0.1% sodium dodecyl sulfate. The amount of DNA in the sample was measured using a fluorometric method described elsewhere [35]. The resulting concentration of DNA was con-

verted to a cell number using an appropriate standard curve relating DNA to cell concentration.

PS and Antibody-targeted Photolysis of FPCLs

FPCLs were cultured for 3 days, washed, incubated with either Bis[$(EtOH)_3N$]-Sn chlorin e6-ethylenediamine (free PS), or immunoconjugate in supplemented DMEM for 16 hr at 37°C, and washed as described for the determination of cellular uptake of mAbs. The lattice was then exposed to an incident beam of light (diameter > 30 mm) delivered by an optic fiber from a 630 nm dye laser (Kiton red was used) pumped by an argon ion laser (both from Coherent, Palo Alto, CA). The average power density was set to 80–100 mW/cm^2. The point to point variation in power density was <10% across the area of the lattice. The irradiation time was varied between 100 sec and 1,000 sec to obtain total light doses between 10 and 100 J/cm^2. The treated FPCLs were returned to the incubator after an additional medium change using supplemented DMEM. For FPCLs overlaid with keratinocytes, the same procedures were followed except that serum-free Keratinocyte Growth Medium was used instead of supplemented DMEM.

Cell Viability Determination

Viability of fibroblasts in FPCLs was determined within 24 hr after light exposure. Calcein AM and ethidium homodimer-1 were added to the culture medium (final concentration: 3 μM and 6 μM, respectively), and after a 30-min incubation at 37°C, the FPCLs were examined by epi-fluorescence microscopy using a 4 X objective. Standard fluorescein and rhodamine filter sets were used to visualize the calcein and ethidium homodimer signals, respectively. Images containing the fluorescence color information were captured with an Optronics VI-470 color CCD camera. Representative image fields from four to ten scattered areas across each FPCL were stored on disk and surviving cell fractions for every FPCL determined by averaging over all fields the ratios of live (calcein stained) to total number of cells (calcein stained plus ethidium homodimer-stained). The viability statistics were evaluated by manual counting of green and red cells in superposed and pseudo-colored images constructed from the two image frames, which were collected at each field position. Image processing software Metamorph (Universal Imaging, West Chester, PA) was used to produce these images. The image superposition permitted automatic correction for any dual counting of the same cell that might have resulted from intense fluorescence bleedthrough from one signal channel to the other. Viability of keratinocytes cultured on the surface of collagen gels as well as FPCLs was determined using the same live/dead stains and techniques. Keratinocytes and fibroblasts could be easily differentiated based on morphology and focal position.

Visualization of Collagen Density

Paired FPCL lattices were identically prepared and exposed to light on the same day using an annular light mask. One member of each pair was evaluated for the spatial dependence of cell viability using the calcein AM/ethidium homodimer bioassay within 24 hr after exposure to light. This was to assure the detection of nuclei from necrotic cells that would have degraded over time. The second member of each pair was then returned to culture for an additional 3 days after light exposure to permit the lattices enough time to further contract. To reveal zonal variations in collagen density within the FPCLs, FPCLs were incubated for 1 hr at room temperature in a solution containing 0.125% w/v Coomassie Blue R-250 in 150 mM NaCl buffered with 10 mM phosphate, pH = 5. Excess dye was removed by serial washes in PBS, buffered at pH 5–6. The lattices were then photographed using light transmission through them as an indicator of collagen density.

RESULTS

Specificity of Photosensitizer

The therapeutic advantage of ATPL for fibroblast removal must be evaluated in terms of its overall cell specificity in comparison with that of the constituent PS. We examined the selectivity of the free PS in FPCLs with fetal foreskin keratinocytes cultured on the top surface. We found that a 4 μM concentration of free PS produces a light dose-dependent cell killing. The dose response curves for this PS have been evaluated for fibroblasts and keratinocytes (Fig. 1). The data do not reveal any significant difference in the sensitivity of the two cell types (ED_{50} for each is ~15 J). Using a 1 μM concentration of free PS, keratinocytes exhibited a greater sensitivity to photolysis compared to fibroblasts. Thus photolysis using free PS cannot achieve selective elimination of fibroblasts while sparing keratinocytes.

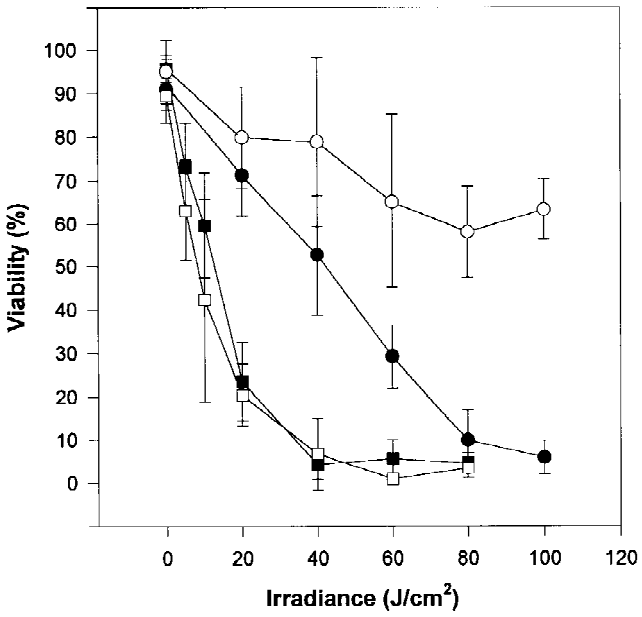

Fig. 1. Dose response of keratinocytes and fibroblasts to free PS. Fibroblasts and keratinocytes were co-cultured for 4 days in FPCLs, incubated with Bis[$(EtOH)_3N$]-SnCe6-ethylenediamine for 16 hr at 37°C. Cell viability was determined 1 day after irradiation. Each point is the average ± SD of at least five different fields. Symbols used are: FPCLs incubated with 1,000 nM PS, (●) keratinocyte viability, (○) fibroblast viability; FPCLs incubated with 4,000 nM PS, (■) keratinocyte viability; (□) fibroblast viability.

Specificity of PR2D3 Antibody

Prior to testing the effect of ATPL on FPCLs, we first characterized the specific uptake of the ^{125}I radiolabeled anti-fibroblast mAb PR2D3 by fibroblasts cultured in FPCLs. FPCLs were incubated with a range of PR2D3 concentrations for 16 hr at 37°C and the amount of cell-associated PR2D3 was determined. PR2D3 uptake increased as a function of the concentration of PR2D3 in the bulk medium (Fig. 2). With 800 nM PR2D3, cell-associated PR2D3 was 5–6-fold higher in 8-day-old compared to 3-day-old FPCLs. In contrast, the uptake of an isotype-matched nonspecific mAb, anti-*P. aeruginosa*, was less than half that of PR2D3 in 3-day-old FPCLs and remained unchanged in the 8-day-old FPCLs. Thus the specific uptake of PR2D3, assumed to be equal to the difference between PR2D3 and anti-*P. aeruginosa* uptakes, was ~50% of the total in 3-day-old FPCLs and 90% in 8-day-old FPCLs. Although specific uptake was higher in 8-day-old FPCLs, the latter had already contracted to a significant extent and could not be used to investigate the effect of ATPL on viability and contraction of FPCLs. For this reason, 3-day-old FPCLs were used in all subsequent experiments.

Viability and Contraction Rate of FPCLs

To demonstrate that ATPL causes specific and dose-dependent killing of fibroblasts in FPCLs, anti-fibroblast (PR2D3) immunoconjugates containing 0.5, 1, and 2 PS/molecule and anti-*P. aeruginosa* immunoconjugates with 1.4, 2.7, and 3.5 PS/molecule were synthesized. The effect of these conjugates, as well as free PS, in combination with various light doses is shown in Table 1. The specific conjugates caused a decrease in cell viability, which increased as a function of light dose and PS loading of the conjugate. Nonspecific conjugates and free PS had little effect on viability, except in cases where the effective PS concentration was 2,000 nM or more, which caused a partial decrease in viability. To establish the specificity of PR2D3 conjugates for fibroblasts, we tested the effect of the PR2D3 conjugate with a loading of 2 PS/molecule on the viability of keratinocytes cultured on top of FPCLs. No significant decrease in viability as a result of ATPL treatment was observed (96 ± 6% and 90 ± 5% pre- and post-ATPL, respectively).

Our prior studies with melanoma cells

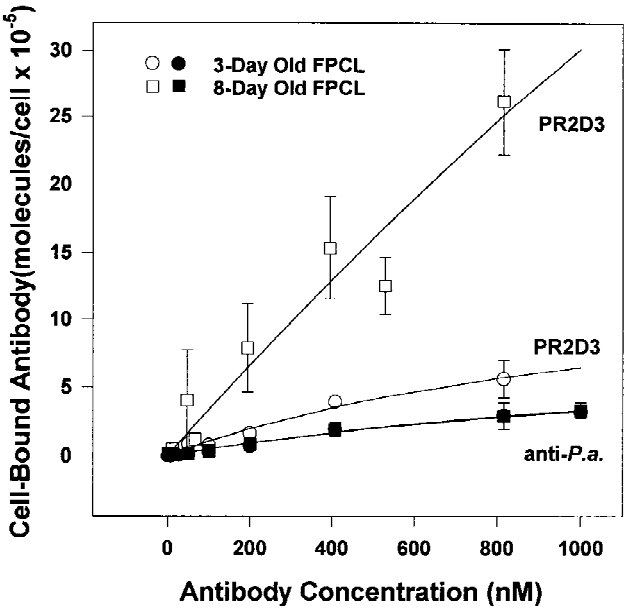

Fig. 2. Uptake of PR2D3 or anti-*P. aeruginosa* by fibroblasts cultured in FPCLs. Fibroblasts were cultured in FPCLs for 3 or 8 days, incubated with radiolabeled antibody for 16 hr at 37°C, and the cell-bound radioactivity determined after retrieving the cells by collagenase digestion of the FPCLs. Data are normalized to cell number based on the DNA content of FPCLs. Each point is the average of triplicate FPCLs ± SD.

TABLE 1. Contraction Rate and Viability of ATPL-treated FPCLs*

Conjugate used	Effective PS concentration ([mAb] × L)[a] (nM)	Number of FPCLs	Light dose (J/cm^2)	Contraction rate (mm/h ± SD)	Viability (% ± SD)
No conjugate	0	6	0	0.12 ± 0.01	95 ± 10
	0	3	160	0.12 ± 0.01	96 ± 5
PS alone	1000	3	0	0.12 ± 0.01	96 ± 3
	1000	2	80	0.06 ± 0.01	78 ± 10
Anti-*P. aeruginosa* conjugate	1400 (1,000 × 1.4)	3	100	0.12 ± 0.01	95 ± 4
	1350 (500 × 2.7)	3	100	0.12 ± 0.01	96 ± 5
	2450 (700 × 3.5)	3	80	0.08 ± 0.01	63 ± 12
PR2D3 conjugate	1000 (1,000 × 1.0)	2	0	0.12 ± 0.01	95 ± 3
	2000 (1,000 × 2.0)	3	0	0.12 ± 0.01	95 ± 7
	500 (1,000 × 0.5)	3	100	0.054 ± 0.005	30 ± 15
	1000 (1,000 × 1.0)	3	100	0.015 ± 0.003	5 ± 3
	1000 (1,000 × 1.0)	2	80	0.020 ± 0.005	9 ± 2
	1000 (1,000 × 1.0)	2	40	0.060 ± 0.006	55 ± 8
	1000 (500 × 2.0)	2	80	0.003 ± 0.005	2 ± 5
	2000 (1,000 × 2.0)	2	80	0.002 ± 0.003	2 ± 2
	2000 (1,000 × 2.0)	3	10	0.057 ± 0.003	65 ± 10

*Three-day-old FPCLs were incubated for 16 hr at 37°C with no conjugate, free PS, specific, or nonspecific immunoconjugates, washed to remove unbound conjugate, and exposed to light. The percentage of surviving fibroblasts 24 hr later was determined by live/dead staining and the contraction rate of the FPCL post-ATPL determined by linear regression of the FPCL diameter vs. time curve over the next 150–250 hr.

[a]Represents product of mAb concentration in medium during incubation times the number of PS/mAb molecule.

showed that the extent of cell killing was correlated with the cumulative phototoxin dose generated by the cell-bound conjugate [24]. Thus we plotted the viability of fibroblasts in FPCLs after ATPL treatment as a function of the calculated singlet oxygen ($^1\Delta_g$) dose generated by cell-associated PR2D3 or anti-*P. aeruginosa* conjugates (Fig. 2). The $^1\Delta_g$ dose is used to normalize the data because it is the most abundant phototoxin generated by the conjugate design used in this study [7,8]. The $^1\Delta_g$ dose per cell was estimated as described previously [8] with the additional correction that PS photobleaching has here been taken into account. The calculation of $^1\Delta_g$ is based on the amount of cell-bound conjugate, the conjugate loading, the total light dose, the quantum yield of $^1\Delta_g$ generation by derivatized Sn(IV) chlorin e_6 (Φ_Δ = 0.80) [10], and the absorption cross section of Sn(IV) chlorin e_6 (2×10^{-20} m^2) [24]. The amount of bound conjugate was determined from the correlation between the concentration of the corresponding mAb and uptake per cell shown in Figure 2. The photobleaching rate constant (β) for this immunoconjugate is constant at $\beta = -.004$ cm^2/J when the oxygen tension is above 0.02 mM [8]. We have used this value to calculate the photobleaching factor [1/β *(1-exp(BJ)], which depends on the light dose (J) received by the sample. The data in Figure 3, which are pooled from experiments using various PR2D3 conjugates and concentrations, appear to follow a common killing curve. Viability decreased monotonically as a function of $^1\Delta_g$ dose until 2×10^{10} molecules/cell, at which point the percentage of viable cells was <5%. A similar viability curve obtained by pooling data from anti-*P. aeruginosa* conjugates shows a slower killing rate at any given $^1\Delta_g$ dose, with viabilities >80% for doses of 2×10^{10} molecules $^1\Delta_g$/cell. Thus for predicted $^1\Delta_g$ doses of ~2×10^{10} molecules/cell, almost complete cell killing is achieved with the specific conjugate, whereas little effect is seen with the nonspecific conjugate.

FPCLs prepared as described in the experimental protocol contracted at a rate of approximately 0.12 mm/hr (Fig. 4A). This rate was constant from the initiation of the experiment until the lattice diameter was reduced to 10–15 mm. In combination with light exposure, the anti-*P. aeruginosa* conjugate did not alter the kinetics of FPCL contraction (Fig. 4B). However, PR2D3 conjugates with 0.5 and 1 PS/molecule inhibited contraction to an increasing degree (Fig. 4C–D), and contraction was virtually halted with a conjugate containing 2 PS/molecule (Fig. 4E). Partial inhibition could be achieved with the latter conjugate if the light dose was decreased from 80 J/cm^2 to 10 J/cm^2 (Fig. 4F). The effect of ATPL on contraction rate was immediate and the resulting contraction rate remained constant until the end of the ex-

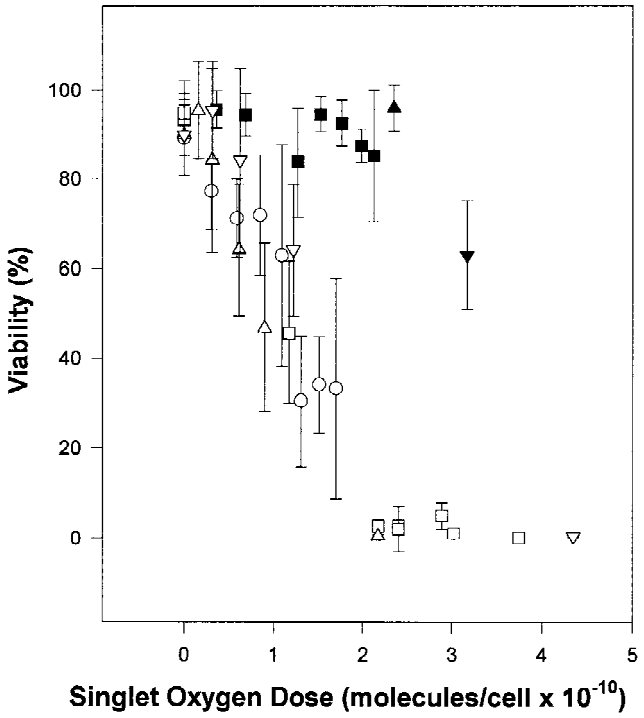

Fig. 3. Effect of phototoxin dose on fibroblast viability in FPCLs. Viability as a function of the predicted $^1\Delta_g$ dose, based on data pooled from several experiments using various combinations of conjugate concentration, PS loading, and light dose. Open and closed symbols are used for PR2D3 and anti-*P. aeruginosa* conjugates, respectively. The symbols represent the following immunoconjugate preparations: (○) 1,000 nM PR2D3, L = 0.5; (□) 1,000 nM PR2D3, L = 1; (△) 500 nM PR2D3, L = 2, (▽) 1,000 nM PR2D3, L = 2; (■) 1,000 nM anti-*P. aeruginosa*, L = 1.4, (▲) 500 nM anti-*P. aeruginosa*, L = 2.7; (▼) 700 nM anti-*P. aeruginosa*, L = 3.5. L = number of PS/mAb molecule.

periment (150–250 hr later). The contraction rates for each FPCL were determined by a least-squares analysis (LSA) of data of mean lattice diameter vs time after ATPL treatment. Those rates were determined for the experiments shown in Figure 4 as well as other conditions listed in Table 1. To establish whether there is a correlation between viability and contraction rate post ATPL, contraction rate was plotted against viability data for experiments using PR2D3 conjugates as well as nonspecific conjugate, PS alone, or no conjugate (Fig. 5). The data indicate that an FPCL contracting at a normal initial rate of 0.12 mm/h exhibits a 90–95% viable cell population. FPCLs that appear to have stopped contracting exhibit a viable cell population of 5% or below. In FPCLs that exhibit 30–80% viability, a ~50% reduction in the original rate of contraction was noted. Overall, the data correlate well with a straight line going through the origin, suggesting a direct proportionality between viability post ATPL treatment and contraction rate.

Spatial Control of Illumination

A useful practical aspect of ATPL is the ability spatially to control the application of light. We imposed a patterned light mask between the light source and the FPCL. In one case, an annulus was placed over the FPCL, thereby allowing irradiation of a circular area 14 mm in diameter in the center of the FPCL. This area roughly corresponds to one-half the total area of the FPCL (overall diameter = 20 mm). Alternatively, a 14 mm circular disk was placed over the FPCL, thereby allowing light to penetrate the outer annulus of the FPCL only. In these experiments, we used 1,000 nM of a PR2D3 conjugate containing 2 PS/molecule and a light dose of 80 J/cm^2. Staining of the FPCLs with calcein and ethidium homodimer shortly after ATPL treatment reveals a sharp transition in viability between the live and dead zones (Figs. 6A,C). Four days after ATPL treatment, similarly treated FPCLs were stained with Coomassie Blue (Figs. 6B,D). Regions containing live cells stained darker, which is indicative of a higher collagen density in those same areas. Overall, contraction rates for ATPL-treated FPCLs with the masks were half that of untreated FPCLs (data not shown), using the same conjugate and light doses. This suggests that fibroblasts in the inner and outer annuli have the potential to contract the lattice at the same radial rate in the absence of light.

DISCUSSION

In this study, we show that antifibroblast mAbs conjugated to PS molecules, when used in combination with light, inhibit the contraction of FPCLs and cause fibroblast killing in a dose-dependent manner. The specificity of this technique is evidenced by (1) the lack of cytotoxic activity against keratinocytes cultured on FPCLs, and (2) the ability to confine fibroblast killing to limited regions of an FPCL via spatial control of illumination. Furthermore, a combination of specific conjugate dose, PS loading, and light dose, which generates a predicted $^1\Delta_g$ dose of ~2×10^{10} molecules/cell, is capable of inducing a nearly complete inhibition of FPCL contraction, whereas a similar dose delivered by a nonspecific conjugate causes little change in these parameters. Cell viability and contraction rate post-ATPL

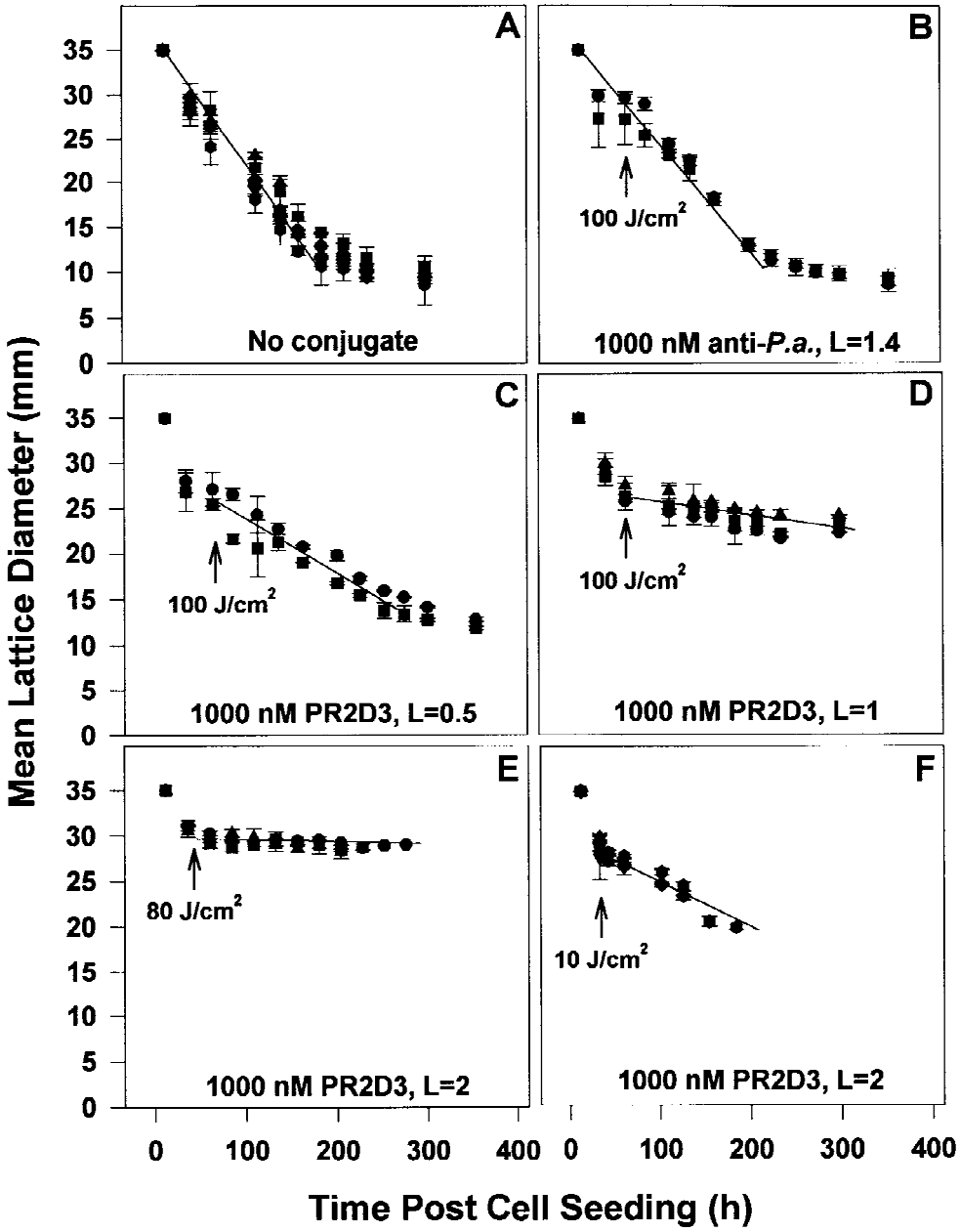

Fig. 4. Effect of ATPL on FPCL contraction. FPCLs were seeded and allowed to contract for 3 days, after which they were incubated with immunoconjugate and exposed to light. FPCL size was then monitored for an additional 10 d. **A:** Control untreated FPCL undergoing contraction. **B:** Control FPCL treated using 1,000 nM of nonspecific anti-*P. aeruginosa* conjugate, L = 1.4, 100 J/cm^2. **C:** FPCL treated with 1,000 nM PR2D3 conjugate, L = 0.5, 100 J/cm^2. **D:** FPCL treated with 1,000 nM PR2D3 conjugate, L = 1, 100 J/cm^2. **E:** FPCL treated with 1,000 nM PR2D3 conjugate, L = 2, 80 J/cm^2. **F:** FPCL treated with 1,000 nM PR2D3 conjugate, L = 2, 10 J/cm^2. The time of application of light is indicated by an arrow in each panel. Each point represents the average diameter of one FPCL measured along two orthogonal directions. Each symbol corresponds to a different FPCL.

treatment were strongly correlated, suggesting that inhibition of contraction is a direct result of ATPL-mediated fibroblast killing. This result is consistent with previous findings demonstrating that FPCL contraction is caused by direct pulling of the collagen fibers by fibroblasts [27,28]. Thus the contraction rate of a FPCL can be modulated in a predictable fashion using ATPL by establishing a relationship between fibroblast viability and phototoxin dose generated.

To target fibroblasts in FPCLs, we have chosen the mAb PR2D3, which binds a surface epit-

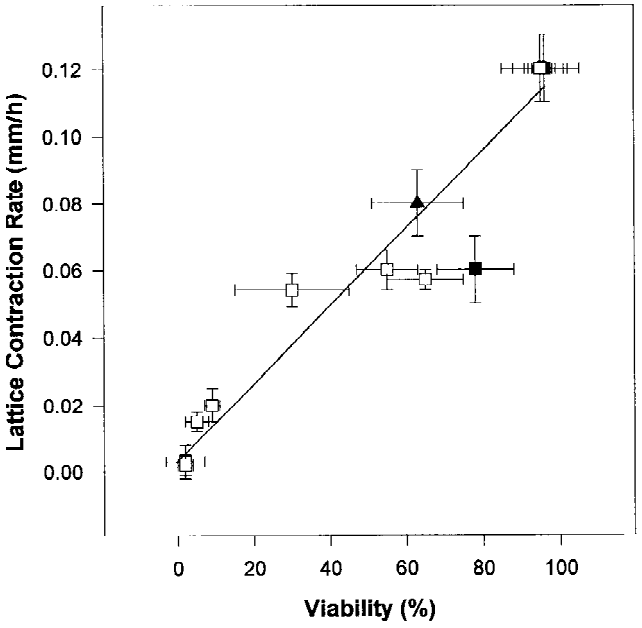

Fig. 5. Correlation between FPCL contraction rate and viability post-ATPL treatment for a variety of combinations of conjugate type, concentration, and loading and light dose. The numerical values of these data and corresponding experimental conditions are summarized in Table 1. Symbols used are: (□) PR2D3 conjugates; (▲) anti-*P. aeruginosa* conjugates; (■) free or no PS. The correlation coefficient for the linear least-squares fit is 0.930.

ope constitutively expressed on cultured smooth muscle cells and myofibroblasts in tissue sections and cross reacts with vascular smooth muscle in the skin [29]. This mAb turned out to be the only one of ten or so different antihuman fibroblast or myofibroblast mAb's targeting cell surface epitopes that we could obtain and that did not cross react with keratinocytes (as determined by our ELISA screening). Although this mAb was found not to bind to CRL 1784 fibroblasts cultured on plastic, the uptake rate of this mAb by the fibroblasts in collagen lattices was significantly higher than that of the nonspecific mAb. Prior studies have shown that fibroblasts cultured in collagen matrices undergo phenotypic changes and express smooth muscle cell actin [3,30]. Uptake of PR2D3 but not that of a nonspecific mAb was greatly enhanced between 3 and 8 days of culture in FPCLs. Thus the induction of the smooth muscle cell phenotype by fibroblasts in FPCLs may lead to an increase in number and/or recycling rate of PR2D3 epitopes on the fibroblast surface.

Interestingly, saturation of the PR2D3 uptake was not apparent at bulk concentrations of mAb of up to 1,000 nM, which is considerably higher than typical specific mAb-antigen binding (~1 nM). Potential explanations include: (1) removal of conjugate from the bulk medium by cellular uptake or degradation, (2) nonspecific binding and uptake mechanisms, and (3) endocytosis and recycling of target epitopes on the cell surface. Depletion of conjugate from the bulk medium due to cellular uptake is unlikely since the total amount of conjugate added to the FPCL (~10^{10} molecules/cell) greatly exceeds the total cellular uptake at 16 hr (~10^6 molecules/cell). One mechanism of nonspecific uptake is fluid phase endocytosis. Typical initial rates in fibroblasts and endothelial cells are 40–50 fL/h/cell [36,37]. Thus for a 16 hr incubation with 1,000 nM of conjugate and assuming no binding of conjugate to the cell, a cumulative uptake of 4–5 × 10^5 molecules of conjugate per cell is theoretically possible. This value is consistent with the uptake of nonspecific conjugate by fibroblasts observed in this study. Microscopic observation of FPCLs incubated with fluorescently labeled specific and nonspecific conjugates revealed the presence of intracellular punctate fluorescence, consistent with internalization of the conjugates (unpub. obs.). The uptake of specific conjugate could be enhanced by receptor mediated endocytosis, e.g., through receptor diffusion to clathrin-coated pits and subsequent invagination into vesicles and endosomes. This is known to be the mechanism of entry of a great number of substances into a variety of cells [38,39]. The association of receptor and coated pit has been modeled as a diffusion controlled process with association/dissociation rate constants for receptors that vary greatly in distinction to the relatively constant rate for invagination of the pits (3.3 × 10^{-3}/s) [39,40]. The rates of internalization of mAb's in fibroblasts differ significantly with the receptor targeted, exhibiting, e.g., endocytosis of 100%/hr of the total surface bound mAb to the α transferrin receptor and <3%/hr of the total surface bound mAb to the c-erbB-2 glycoprotein (homologous to the epidermal growth factor receptor found in human breast cancer cells), which had been transfected into several rat fibroblast lines [41]. Consequently, endocytosis may be an important toxicity enhancement mechanism for future in vivo applications of antibody-targeted therapies. This suggests that higher amounts of cell-associated conjugate can be obtained by using conjugate concentrations that are considerably higher than expected to reach saturation of specific binding sites on the cell surface.

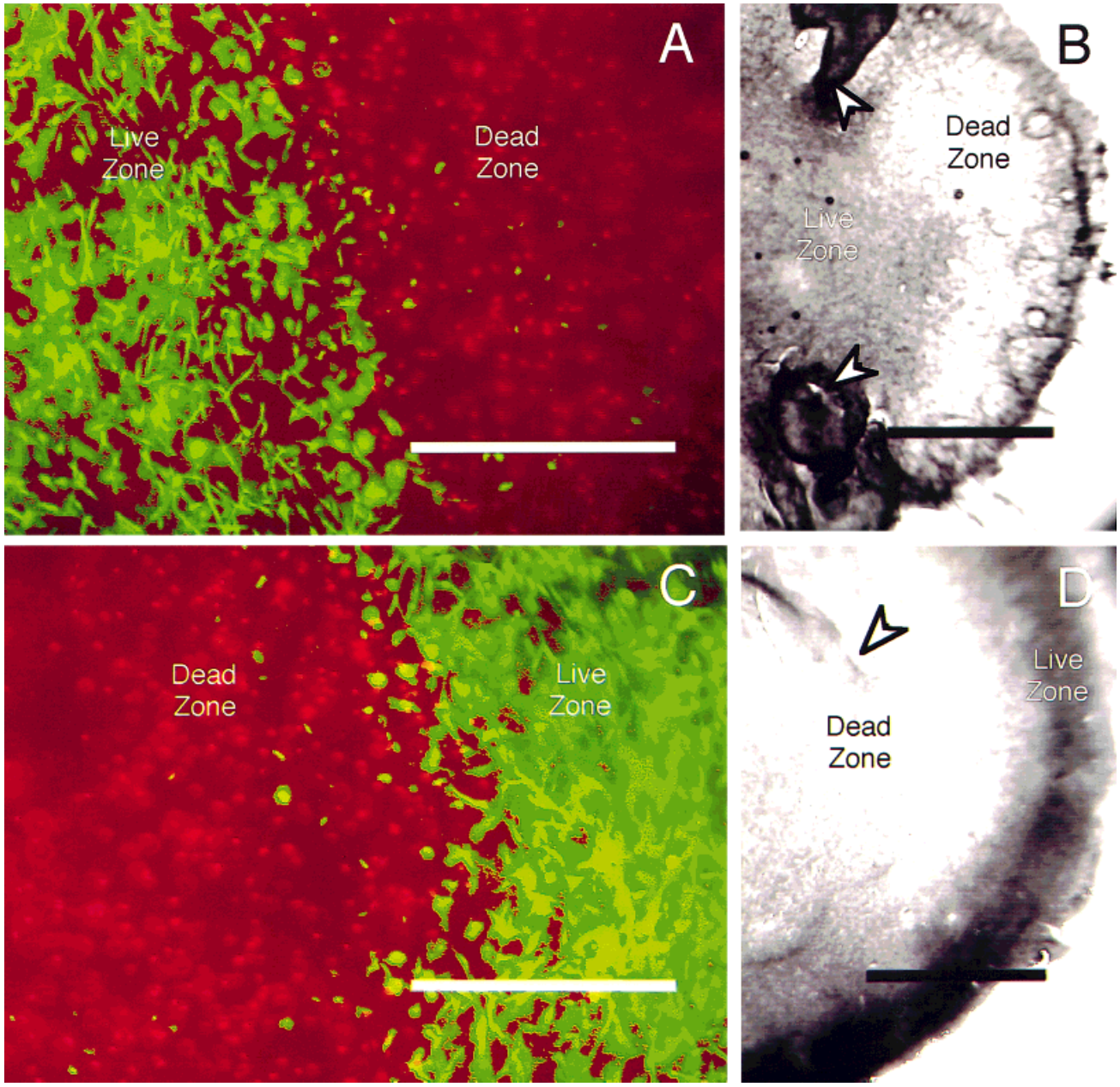

Fig. 6. Effect of an annular mask on the distribution of fibroblast viability and collagen density in FPCLs. A 14 mm annular mask (**A** and **B**) or a 14 mm circular mask were placed over the FPCL (**C** and **D**). Twenty-four hours after irradiation with 100 J/cm^2, staining for live and dead cells was performed. FPCLs were also stained by Coomassie Blue to visualize collagen density. Panels A and C show epifluorescence images acquired 1 day after ATPL treatment. A sharp transition between live (green) and dead (red) zones is easily seen and corresponds to the edge of the mask. The white scale bar corresponds to 1 mm. Panels B and D show the difference in Coomassie Blue staining between regions where collagen was highly compacted by the cells and areas where cells had been killed by ATPL. Arrowheads in B and D indicate areas where the collagen is buckling as a result of unequal contraction rates in the live and dead zones of the FPCL. The black scale bar corresponds to 4 mm.

In the case of FPCLs treated with the PR2D3 conjugate, the cell survival data indicate that cellular damage scales with the predicted $^1\Delta_g$ dose, which depends on the product of the light dose, amount of cell-associated conjugate, conjugate loading, and a photobleaching factor. Thus the same fibroblast killing generated using high concentrations of PS and modest light doses could be achieved by increasing the light exposure to cells incubated with lower concentrations of PS. This finding is consistent with our previous observations with SK-MEL-2 human malignant mela-

noma cells that suggest that photodamage depends on the total phototoxin dose [24]. The viability appears to decrease less rapidly as a function of predicted $^1\Delta_g$ dose per cell for FPCLs treated with the nonspecific anti-*P. aeruginosa* conjugate than for FPCLs treated with PR2D3 conjugates. One potential reason for this discrepancy is that the uptake data, which were obtained with the mAbs not conjugated to $SnCle_6$, may not reflect the uptake of conjugated mAbs. However, this is unlikely since we have previously shown that the conjugation technique via the oligosaccharide moiety of the Fc fragment does not significantly affect the binding behavior of the mAb [10]. Alternatively, the difference could be related to a distinct compartmentalization of specific and nonspecific conjugates in or on the target cell. This difference could alter the yield or capture probability of $^1\Delta_g$ or other phototoxins and alter the distance between critical cellular structures and the PS. For example, if intracellular PS is sufficiently proximal to endogeneous electron donors such as NADH, photoactivated transfer of electrons to the PS could occur [8]. In the presence of oxygen, each electron transfer generates one molecule of superoxide, which could indirectly cause additional radical damage to the cell.

The contraction rate also could be modulated by imprinting arbitrary patterns of necrotic and viable fibroblasts into the collagen matrix with the aid of a light mask. The fact that collagen lattices intensely scatter the activating light limits, in theory, the spatial confinement of necrosis one can actually achieve. However, there was a clear demarcation between live and dead zones, with a relatively narrow intermediate annular zone with both live and dead cells ~0.2 mm wide. We observed that Coomassie Blue stained regions of live cells darker than light exposed areas of the lattices, indicating that collagen contraction was specifically inhibited in ATPL-treated regions. Thus spatial control of the illumination may be efficiently used to limit cell killing and inhibition of collagen contraction to specific areas.

The PS used, Sn(IV) chlorin e_6, has a strong absorbance within the therapeutic window (600–1,300 nm), excellent photostability, a high quantum yield for $^1\Delta_g$ generation in the absence of electron donors, and a small rate constant for photobleaching [8,24,31]. Based on our finding that the PR2D3-Sn(IV) chlorin e_6 conjugate can inhibit FPCL contraction in vitro, we envision that the same conjugate may be useful to control the contraction rate of open wounds and prevent or inhibit the formation of abnormal scars (i.e., keloids and hypertrophic scars). A priori, ATPL could have several advantages over current techniques to treat hypertrophic scars: (1) assuming that PR2D3 lacks cross-reactivity with keratinocytes in vivo, it would target the putative agents of wound contraction (fibroblasts and myofibroblasts) without affecting the regenerating epithelium, and (2) it would enable one spatially to limit the treatment area, thereby limiting systemic and other undesirable side effects. We have recently shown that the same PR2D3 conjugates used in this study have the ability to inhibit the growth of human hypertrophic scar tissue implanted in nude mice [26]. We also have recently found that these conjugates effectively destroy keloid fibroblasts (ATCC 1762-CRL) cultured in collagen lattices (unpub. obs.). The primary advantage of this antibody is that it does not cross react with keratinocytes, which are an essential restorative element in wound healing. They occupy the most superficial layer of skin and would therefore experience the greatest irradiance and hence exhibit the greatest susceptibility to damage during photodynamic therapy. The potential cross-reactivity of PR2D3 with vascular smooth muscle cells may, however, limit its usefulness in therapeutic applications. Nevertheless, this immuno-conjugate illustrates the potential usefulness of ATPL directed against fibroblasts as a tool to modulate the wound healing process.

In conclusion, we have demonstrated that antifibroblast-Sn(IV) chlorin e_6 conjugates, when used in combination with light, can efficiently control the contraction rate of FPCLs. The contraction rate post-ATPL is linearly related with the percentage of remaining viable cells. The percentage of cells killed by ATPL scaled with the predicted $^1\Delta_g$ dose, a function of the light dose, conjugate concentration, conjugate loading, and a correction factor to account for photobleaching. Thus, ATPL is a promising and versatile technique to control the process of ECM remodeling by connective tissue cells and has potential therapeutic applications in wound healing in vivo.

ACKNOWLEDGMENTS

This work was supported by the Shriners Hospitals for Crippled Children and the Lucille P. Markey Charitable Trust.

REFERENCES

1. Rockwell WB, Cohen IK, Ehrlich HP. Keloids and hypertrophic scars: A comprehensive review. Plas Reconstr Surg 1989; 84:827–837.
2. Ahn S-T, Monafo WW, Mustoe TA. Topical silicone gel for the prevention and treatment of hypertrophic scar. Arch Surg 1991; 126:499–504.
3. Rudolph R, Vande Berg J, Ehrlich HP. Wound contraction and scar contracture. In: Cohen, IK, and Diegelmann, eds. "Wound Healing, Biochemical and Clinical Aspects." Philadelphia: W.B. Saunders, 1992: 96–114.
4. Bell E, Ivarsson B, Merrill C. Production of a tissue-like structure by contraction of collagen lattices by human fibroblasts of different proliferative potential in vitro. Proc Natl Acad Sci 1979; 76:1274–1278.
5. Bell E, Sher S, Hull B, Merrill C, Rosen S, Chamson A, Asselineau D, Dubertret L, Coulomb B, Lapiere C, Nusgens B, Neveux Y. The reconstitution of living skin. J Invest Dermatol 1983; 81:2s–10s.
6. Friedberg JS, Tompkins RG, Rakestraw SL, Warren SW, Fischman AJ, Yarmush ML. Antibody-targeted photolysis. Bacteriocidal effects of Sn(IV) chlorin e_6-dextran-monoclonal antibody conjugates. Ann NY Acad Sci 1991; 618:383–393.
7. Strong L, Lu X-M, Tompkins RG, Yarmush ML. Bacterial cell killing by antibody targeted photolysis: Enhanced effect by OH radical generation. J Contr Rel 1994; 28:175–186.
8. Strong LH, Yarmush D, Yarmush ML. Antibody targeted photolysis: Photophysical, biochemical, and pharmacokinetic properties of anti-bacterial conjugates. Ann NY Acad Sci 1994; 745:297–320.
9. Berthiaume F, Reiken SR, Toner M, Tompkins RG, Yarmush ML. Antibody-targeted photolysis of bacteria in vivo. Biotechnol 1994; 12:703–706.
10. Lu X-M, Fischman AJ, Stevens E, Lee TT, Strong LH, Tompkins RG, Yarmush ML. Sn-chlorin e6 antibacterial immunoconjugates: An in vitro and in vivo analysis. J Immunol Meth 1992; 156:85–99.
11. Mew D, Wat CK, Towers GHN, Levy JG. Photoimmunotherapy: treatment of animal tumors with tumor specific monoclonal antibody-hematoporphyrin conjugate. J Immunol 1983; 130:1473–1477.
12. Mew D, Lum V, Wat CK, Towers GHN, Sin CHC, Walter RJ, Wright W, Berns MW, Levy JG. Ability of specific monoclonal antibodies and conventional antisera conjugated to hematoporphyrin to label and kill selected cell lines subsequent to light activation. Cancer Res 1985; 45:4380–4386.
13. Oseroff AR, Ohuoha D, Hasan T, Bommer JC, Yarmush ML. Antibody-targeted photolysis: Selective photodestruction of human T-cell leukemia cells using monoclonal antibody-chlorin e6 conjugates. Proc Natl Acad Sci USA 1986; 83:8744–8748.
14. Yemul S, Berger C, Estabrook A, Suarez S, Edelson R, Bayley H. Selective killing of T lymphocytes by phototoxic liposomes. Proc Natl Acad Sci USA 1987; 84:246–250.
15. Steele JK, Liu D, Stammers AT, Whitney S, Levy JG. Suppressor deletion therapy: Selective elimination of T suppressor cells in vivo using a hematoporphyrin conjugated monoclonal antibody permits animals to reject syngeneic tumor cells. Cancer Imunol Immunother 1988; 26: 125–131.
16. Morgan J, Gray AG, Huehns ER. Specific targeting and toxicity of sulphonated aluminum phtalocyanine photosensitized liposomes directed to cells by monoclonal antibody in vitro. Br J Cancer 1989; 59:366–370.
17. Hasan T, Lin A, Yarmush D, Oseroff A, Yarmush ML. Monoclonal antibody-chromophore conjugates as selective phototoxins. J Controlled Rel 1989; 10:107–117.
18. Hasan T, Lin CW, Lin A. Laser induced selective cytotoxicity using monoclonal antibody chromophore conjugates. Prog Clin Biol Res 1989; 33:627–634.
19. Jiang FN, Jiang S, Liu D, Richter A, Levy JG. Development of technology for linking photosensitizers to a model monoclonal antibody. J Immun Meth 1990; 34:139–149.
20. Jiang FN, Liu DJ, Neydorff H, Chester M, Jiang SY, Levy JG. Photodynamic killing of human squamous cell carcinoma cells using a monoclonal antibody-photosensitizer conjugate. J Natl Can Inst 1991; 83:1218–1225.
21. Jiang FN, Levy JG. Efficacy of photodynamic killing with membrane associated and internalized monoclonal antibody-photosensitizer conjugate. Photochem Photobiol 1991; 54:65–75.
22. Rakestraw SL, Tompkins RG, Yarmush ML. Antibody targeted photolysis: in vitro studies with Sn(IV) chlorin e6 covalently bound to monoclonal antibodies using a modified dextran carrier. Proc Natl Acad Sci USA 1990; 87:4217–4221.
23. Rakestraw SL, Tompkins RG, Yarmush ML. Preparation and characterization of immunoconjugates for antibody targeted photolysis. Bioconj Chem 1990; 1:212–221.
24. Rakestraw SL, Ford W, Tompkins RG, Rodgers MAJ, Thorpe WP, Yarmush ML. Antibody targeted photolysis: immunological, photophysical, and selective phototoxic properties of monoclonal antibody-dextran-Sn(IV) chlorin e6 covalent immunoconjugates. Biotechnol Prog 1992; 8:30–39.
25. Thorpe WP, Toner M, Ezzell RM, Tompkins RG, Yarmush ML. Dynamics of photoinduced cell membrane injury. Biophys J 1995; 68:1–9.
26. Wolfort S, Reiken SR, Berthiaume F, Tompkins RG, Yarmush ML. Monoclonal antibody targeted photolytic control of hypertrophic scar growth in the nude mouse. J Surg Res 1996; 62:17–22.
27. Harris AK, Wild P, Stopack D. Silicone rubber substrata: A new wrinkle in the study of cell locomotion. Science 1980; 208:177–179.
28. Ehrlich HP, Rockwell WB, Cornwell TL, Rajaratnam JBM. Demonstration of a direct role for myosin light chain kinase in fibroblast-populated collagen lattice contraction. J Cell Physiol 1991; 146:1–7.
29. Richman PI, Tilly R, Jass JR, Bodmer WF. Colonic pericrypt sheath cells: Characterization of cell type with new monoclonal antibody. J Clin Pathol 1987; 40:593–600.
30. Desmouliere A, Rubbia-Brandt L, Grau G, Gabbiani G. Heparin induces α-smooth muscle actin expression in cultured fibroblasts and in granulation tissue myofibroblasts. Lab Invest 1992; 67:716–726.
31. Parrish JA. New concepts in therapeutic photomedicine: Photochemistry, optical targeting and the therapeutic window. J Invest Dermatol 1981; 77:45–50.
32. Eskinaz DP, Eby WC, Molinaro GA. Screening of monoclonal antibodies to human cellular and soluble antigens. Meth Enzymol 1986; 121:783–796.

33. Dunn JCY, Tompkins RG, Yarmush ML. Long-term in vitro function of adult hepatocytes in a collagen sandwich configuration. Biotechnol Prog 1991; 7:237–245.
34. Bolton AF, Hunter WM. The labelling of proteins to high specific radioactivities by conjugation to a ^{125}I-containing acylating agent. Biochem J 1973; 133:529–539.
35. Downs TR, Wilfinger WW. Fluorometric quantitation of DNA in cells and tissue. Anal Biochem 1983; 131:538–547.
36. Schroeder F. Altered phospholipid composition affects endocytosis in cultured LM fibroblasts. Biochim Biophys Acta 1981; 649:162–174.
37. Davies PF, Selden III SC, and Schwartz SM. Enhanced rates of fluid phase pinocytosis during exponential growth and monolayer regeneration by cultured arterial endothelial cells. J Cell Physiol 1980; 102:119–127.
38. Goldstein JL, Anderson RGW, Brown MS. Coated pits, coated vessicles, and receptor mediated endocytosis. Nature (Lond) 1979; 279:679–685.
39. Goldstein B, Wofsy C, Bell G. Interactions of low density lipoprotein receptors with coated pits on human fibroblasts: estimate of the forward rate constant and comparison with the diffusion limit. Proc Natl Acad Sci, USA 1981; 78:5695–5698.
40. Keizer J, Ramirez J, Peacock-Lopez E. The effect of diffusion on the binding of membrane-bound receptors to coated pits. Biophys J 1985; 47:79–88.
41. Maier LA, Xu TJ, Hester S, Boyer CM, McKenzie S, Bruskin AM, Argon Y, Bast Jr RC. Requirements for the internalization of a murine monoclonal antibody directed against the HER-2/neu gene product c-erbB-2. Cancer Res. 1991; 51:5361–5369.